OPEN

Synergistic effect of Brønsted acid and platinum on purification of automobile exhaust gases

Wei Fu[1], Xin-Hao Li[1], Hong-Liang Bao[2], Kai-Xue Wang[1], Xiao Wei[1], Yi-Yu Cai[1] & Jie-Sheng Chen[1]

[1]School of Chemistry and Chemical Engineering, Hirano Institute for Materials Innovation, Shanghai Jiao Tong University, Shanghai 200240, China, [2]Shanghai Synchrotron Radiation Facilities, Shanghai Institute of Applied Physics, Chinese Academy of Sciences, Shanghai 201204, China.

The catalytic purification of automobile exhaust gases (CO, NO_x and hydrocarbons) is one of the most practiced conversion processes used to lower the emissions and to reduce the air pollution. Nevertheless, the good performance of exhaust gas purification catalysts often requires the high consumption of noble metals such as platinum. Here we report that the Brønsted acid sites on the external surface of a microporous silicoaluminophosphate (SAPO) act as a promoter for exhaust gas purification, effectively cutting the loading amount of platinum in the catalyst without sacrifice of performance. It is revealed that in the Pt-loaded SAPO-CHA catalyst, there exists a remarkable synergistic effect between the Brønsted acid sites and the Pt nanoparticles, the former helping to adsorb and activate the hydrocarbon molecules for NO reduction during the catalytic process. The thermal stability of SAPO-CHA also makes the composite catalyst stable and reusable without activity decay.

T he simultaneous catalytic removal of major pollutants CO, NO_x and hydrocarbons (HCs) from the exhaust gases of a gasoline engine is an important conversion process to reduce the emissions of toxic gases from automobiles. Platinum-containing catalysts have attracted increasing attention in the past decades because of their superior activity as a catalyst not only for redox reactions but also for purification of automobile exhaust gases[1–5]. Many researches have been focused on the development of Pt-loaded catalysts that are desired to effectively eliminate the emission of harmful gases under practical operation conditions[4]. Despite great efforts to date with significant successes, the good performance of catalysts usually leads to high consumption of expensive noble metals, and recovery of noble metals from spent catalysts is required. In general, the performance of a catalyst is also heavily dependent on the physical and chemical properties of its support, which should possess not only a considerable surface area to sustain a uniform dispersion of noble metals, but also strong interaction with the metals to promote the redox reactions[6]. In this context, the selection of suitable supports is very critical in determining the performance and the cost of Pt-containing catalysts for purifying emission gases.

To optimize catalyst supports for stabilizing Pt nanoparticles, materials that allow access to activating substrates and/or elevating the activity of Pt nanoparticles are preferred. Microporous crystalline silicoaluminophosphates (SAPOs) are an important class of molecular sieve materials which have been widely used in adsorption, separation and catalysis. Among the SAPOs, chabazite-type SAPO (SAPO-CHA)[7] with small pores and fairly strong Brønsted acidity has shown excellent catalytic activity and shape selectivity in methanol-to-olefin (MTO) conversion[8–10] and HC transformation[11–13]. It is thus rather promising to integrate the catalytic activity of SAPO-CHA with rich Brønsted acid sites and Pt nanoparticles for efficient removal of automobile exhaust gases, which also contain HCs, under even mild conditions. Although previous studies have used SAPO-CHA containing metal cations for removal of NO_x through a selective-catalytic-reduction (SCR) pathway[14–16], the exploitation of rich Brønsted acid sites in SAPO-CHA support for activating noble metal nanoparticles to simultaneously purify the major pollutants CO, NO_x and HC of a gasoline engine emission has not been described yet. In this report, we demonstrate the remarkable promotion effect of Brønsted acid sites of SAPO-CHA on the catalytic performance of supported Pt catalyst for purification of automobile exhaust gases. Accordingly, the catalyst cost may be reduced markedly by decreasing the Pt-loading amount on the SAPO-CHA material without sacrifice of catalytic performance.

Results

Preparations of catalysts. We prepared the microporous SAPO-CHA with a crystal size of 1.02 μm and an outer surface area of 32 $m^2 g^{-1}$ through a typical hydrothermal route (see Methods). An aluminophosphate analogue

(AlPO-CHA) with similar CHA framework structure (Fig. S1) was also prepared as Brønsted acid-free reference material[17,18]. In SAPO-CHA, a part of the PO_4 tetrahedra are replaced by SiO_4 units, resulting in negative charges which may be balanced by extra-framework protons, that is, Brønsted acid sites discussed in this work. Pt nanoparticles were loaded on the surface of AlPO-CHA and SAPO-CHA through an impregnation approach, and the resulting materials are designated as Pt/AlPO-CHA and Pt/SAPO-CHA, respectively. For comparison, a Pt-loaded alumina material (Pt/Al$_2$O$_3$) was also prepared similarly and used as a reference. Pt nanoparticles were mainly dispersed on the external surface of the molecular sieves as the size of Pt nanoparticles observed in the TEM image (Figure S2) is much larger that the pore size of the molecular sieves.

Distribution of Brønsted acid sites. The distribution of Brønsted acid sites was initially investigated by temperature-programmed desorption (TPD) measurements (Fig. 1a), where NH_3 and pyridine were used as the probe molecules. The NH_3–TPD profiles with two strong desorption peaks at temperatures of 680 and 850 K reveal a rich amount of Brønsted acid sites on the surface of SAPO-CHA based materials and also the Brønsted-acid-free nature of AlPO-CHA materials (Figure 1a). This observation has been doubly confirmed by the Fourier transform infrared (FTIR) spectra of dehydrated SAPO-CHA with strong absorptions at 3630 and 3600 cm^{-1} (Fig. S3). Pyridine molecules with a large dynamic diameter (0.65 nm) cannot diffuse into the micropores (window size 0.43 nm) of SAPO-CHA, and were thus used as probe molecules to characterize the acidity of the external surfaces of SAPO-CHA. The strong signal at 1540 cm^{-1}, arising from protonated pyridinium cations, in the FTIR spectrum (Fig. 1b) of pyridine-adsorbed samples indicates a substantial amount of Brønsted acid sites on the external surface of SAPO-CHA, whilst such a signal disappeared in the spectra of Brønsted-acid-free AlPO-CHA.

Chemical state of the Pt on the surface of various supports. The Pt nanoparticles are believed to be highly active in many important catalytic reactions as compared with their oxide PtO_2[19,20]. For conventional Pt-containing catalysts (e.g. Pt/Al$_2$O$_3$), a pre-activation process to reduce the PtO_2 component to metallic Pt has to be conducted at an elevated temperature before practical use and/or reuse, resulting in additional cost due to the consumption of H_2 gas and electric energy. The stability of the metallic Pt should also be seriously considered in designing new sustainable catalysts. Both the X-ray absorption near-edge structure (XANES) spectra (Figure S4) and Fourier transformed extended X-ray absorption fine structure (EXAFS) spectra (Figure 1c) of the Pt species dispersed on SAPO-CHA and AlPO-CHA are similar to those of Pt foil, rather speaking for the formation of metallic Pt nanoparticles. As described previously, the Pt species on Al$_2$O$_3$ exist mainly as Pt oxide[21,22]. The representative schematic illustrations for the Pt species dispersed on different supports are shown in the inset of Fig. 1c. It can be envisaged that the nature of the support gives a significant impact on the state of Pt species generated on the support. No obvious reduction peaks were observed for Pt/SAPO-CHA and Pt/AlPO-CHA materials in the temperature-programmed reduction (TPR) experiments (Fig. S5), and this is to say that the high-temperature activation process in H_2 is not essential for Pt/SAPO-CHA catalyst. It is thus quite convenient for Pt/SAPO-CHA to be directly used in purification of automobile exhaust gases.

The catalytic performance. The catalytic activities of the Pt-loaded materials were tested in the purification of the exhaust gases of a gasoline engine. The conversions of exhaust gases (NO, CO and
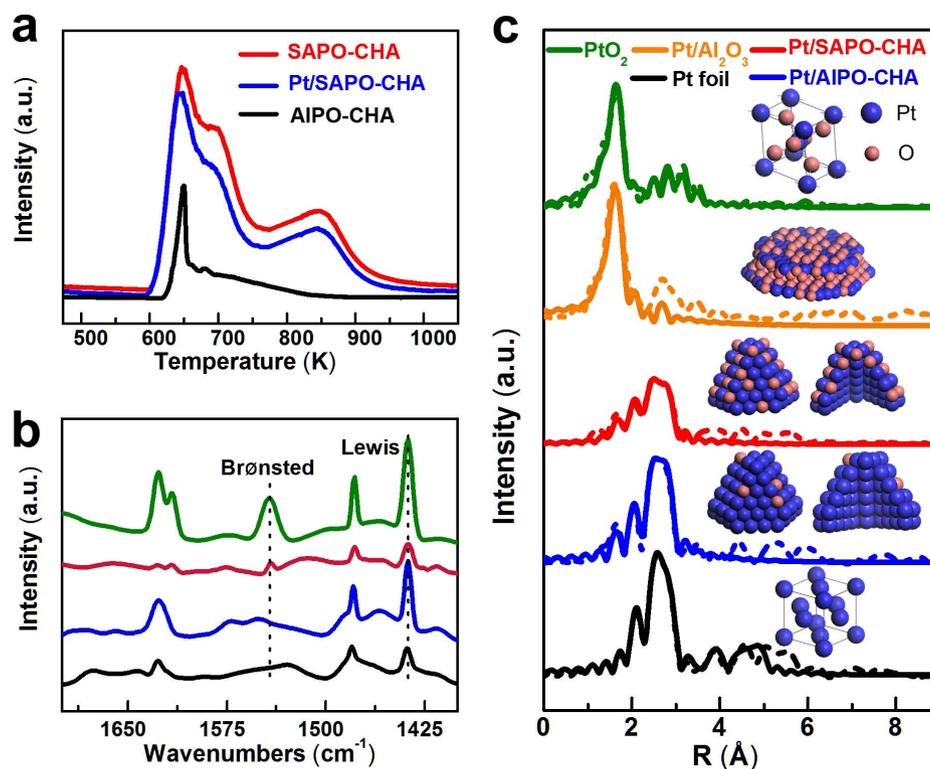
Figure 1 | General characterization of Pt/AlPO-CHA, Pt/SAPO-CHA and Pt/Al$_2$O$_3$. (a) NH_3-TPD profiles. There are rich Brønsted acid sites on the internal and external surfaces of the as-prepared Pt/SAPO-CHA, while no such sites exist in the Pt/AlPO-CHA material. (b) FTIR spectra of pyridine-adsorbed SAPO-CHA outgased at 573 K (red) and 373 K (green) and AlPO-CHA outgased at 573 K (black) and 373 K (blue). (c) Fourier-transformed EXAFS spectra (solid lines) along with theoretical fits (dashed lines), which indicate that the Pt species on SAPO-CHA and AlPO-CHA are mainly metal nanoparticles, whereas on Al$_2$O$_3$ they are mainly Pt oxide. a.u. = arbitrary units.

C_3H_6) over Pt/SAPO-CHA and control catalysts were monitored at gradually increased reaction temperatures. Previously, C_3H_6 has been widely applied as a typical model of HCs to evaluate the catalytic performance of catalysts in purification of automobile exhaust gases, and it was thus used in this work accordingly. As shown in Figure 2, the conversions of C_3H_6, NO and CO over Pt/SAPO-CHA are all higher than those of Pt/AlPO-CHA and Pt/Al$_2$O$_3$ with the same Pt-loading content (0.5 wt%). The temperature at a conversion of 50% of C_3H_6 over Pt/SAPO-CHA is 549 K, nearly 100 and 50 K lower than that over Pt/Al$_2$O$_3$ and Pt/AlPO-CHA respectively (Fig. 2), while the temperature at a conversion of 90% of C_3H_6 is about 578 K for Pt/SAPO-CHA, also much lower than those of Pt/AlPO-CHA (630 K) and Pt/Al$_2$O$_3$ (655 K). Moreover, bare SAPO-CHA as the catalyst gave no conversion of C_3H_6, NO and CO, suggesting that only Pt particles acted as the active cites for such a catalytic reaction. The turnover frequencies (TOF) over Pt/SAPO-CHA were calculated to be 0.014, 0.019 and 0.217 s^{-1} respectively for C_3H_6, NO and CO at a temperature of 575 K. These TOF values are distinctly higher than those of all the other catalysts (including the Pt/Al$_2$O$_3$-aging material) used in this work, and than those of Pt-, Pd-, or Rh-NPs based catalysts reported in the literature under similar conditions (Table S1)[23–27]. Furthermore, products of NO conversion have been identified through gas chromatograph (GC) and gas-phase FTIR measurements. As shown in Figure S6, typical IR bands of N_2O gas at 2212 and 2235 cm^{-1} were detected in the spectra of products catalyzed over Pt/AlPO-CHA and Pt/Al$_2$O$_3$, showing the moderate selectivity of these catalysts. The fact that the peaks of N_2O gas were not present in the spectra of purified gases over Pt/SAPO-CHA reveals the high selectivity of this catalyst in the purification of exhausting gases, again speaking for the advantage of SAPO-CHA as the catalyst support here.

The content of Pt loaded also affects the catalytic performance of the resulting catalysts to a considerable extent (Fig. S7). The activity of the catalysts increased with increasing amount of Pt components. It is noteworthy that the catalytic performance of Pt/SAPO-CHA with a Pt loading as low as 0.25 wt% is comparable with that of Pt/Al$_2$O$_3$ with a Pt loading as high as 1.0 wt%. As an excellent catalyst support, SAPO-CHA can significantly reduce the amount of the noble metal Pt and thus the cost of the catalyst.

Discussion

To find out how the Brønsted acid affects the catalytic activity, it is essential to understand the nature of the acid sites in the SAPO-CHA molecular sieve. Individual Brønsted acid site is a hydroxyl proton located at bridging oxygen between tetrahedrally coordinated silicon and aluminum atoms (Figure 3b). Previous studies indicated that adsorption of olefins (e.g. C_3H_6 here) on Brønsted acid sites tend to be transformed to alkoxy species with a carbeniumion-like feature, which can undergo further reactions to become other derivative

products in various task-specific catalytic reactions[28–30]. We thus calculated the structure of the SAPO-CHA using relativistic density functional theory (DFT) to elucidate the function of Brønsted acid in the catalytic transformation of C_3H_6. The simulation results suggest a very high electron density around the Brønsted acid sites (Fig. 3b), which facilitates the adsorption and activation of C_3H_6 molecules for conversion into covalent alkoxy species in the catalytic reactions[31]. Moreover, the high electron density of the Pt nanoparticles will also be enhanced once Pt nanoparticles form a contact at the electron-rich surface of SAPO-CHA, promising a possibility to improve the catalytic activity of Pt nanoparticles. The facts that the bare SAPO-CHA with rich Brønsted acid sites offered no obvious activity for purifying exhaust gases (Figure S7) and gave much better catalytic performance as catalyst support than that of Brønsted-acid-site-free AlPO-CHA reveals an obvious synergistic effect between the Brønsted acid sites and the Pt nanoparticles. Such a synergistic effect facilitates conversion of C_3H_6 and NO gases via simultaneously lowering the energy barrier of the oxidation reaction of HCs and enhancing the activity of Pt nanoparticles (Fig. 3c, Supplementary Movie S1).

On the basis of our experimental and calculation results in combination with the observations reported in the literature[32–35], a catalytic cycle for the exhaust gas purification reaction over the Pt/SAPO-CHA catalyst is proposed and depicted in Fig. 3d. First, the C_3H_6 molecules are attracted by the Brønsted acid sites (step i), followed by conversion into covalent alkoxy species (step ii). These species are oxidized by O_2 over adjacent Pt nanoparticle, leading to the formation of acetate, H_2O, and CO_2 (step iii, iv). The acetate further react with NO to form nitrogen-containing organic intermediates (step v), which are further converted via formate (step vi) and HNCO species and finally into N_2 and CO_2 by following the reaction of $NCO^- + NO = N_2 + CO_2$ (step vii).

Reusability of the Pt/SAPO-CHA catalysts is another important aspect for practical application. To enhance the stability and thus keep the activity of Pt-nanoparticle based catalysts, the morphology and composition of the as-formed Pt nanoparticles should be maintained during catalytic reactions. The advantage of SAPO-CHA over the conventional γ-Al$_2$O$_3$ as a catalyst support to prevent the metallic Pt from oxidation has been demonstrated earlier in this communication, and is also confirmed by HRTEM analysis (Figure S8). It is found that the SAPO-CHA as well as AlPO-CHA with abundant PO$_4$ tetrahedra in the framework and the external surface (Fig. S9) can act as efficient stabilizer to improve the homogeneous dispersion of Pt nanoparticles and keep them from agglomeration during reactions (Fig. S8).

The thermal and chemical stability of catalyst supports is equally important to ensure their reusability. The structure and crystallinity of SAPO-CHA remains unchanged after reaction as confirmed by the FTIR (Fig. S9) and XRD (Fig. S10) analysis. As conventional catalysts for hydrogen transformation, zeolitic catalysts, including SAPO-CHA
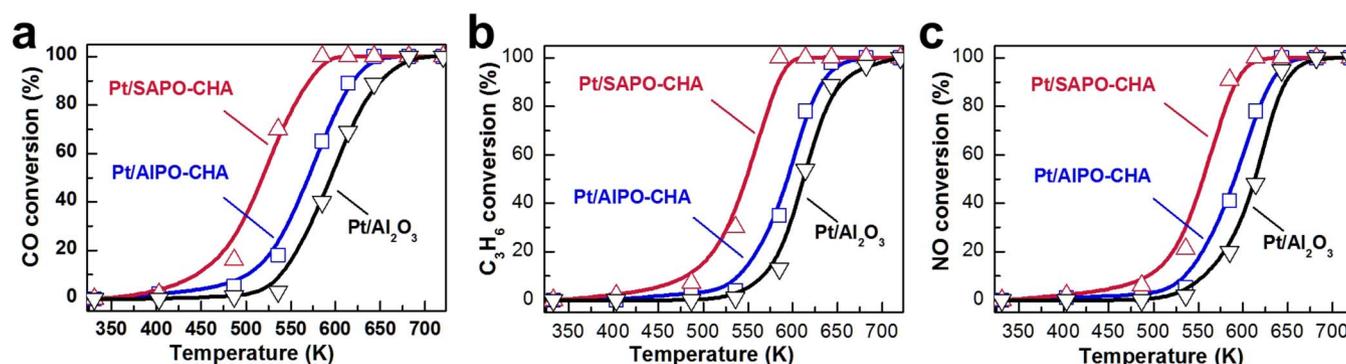
Figure 2 | Catalytic performances of Pt/AlPO-CHA, Pt/SAPO-CHA and Pt/Al$_2$O$_3$ with the same Pt content of 0.5 wt%. (a) Conversion of CO, (b) conversion of C_3H_6, and (c) conversion of NO.
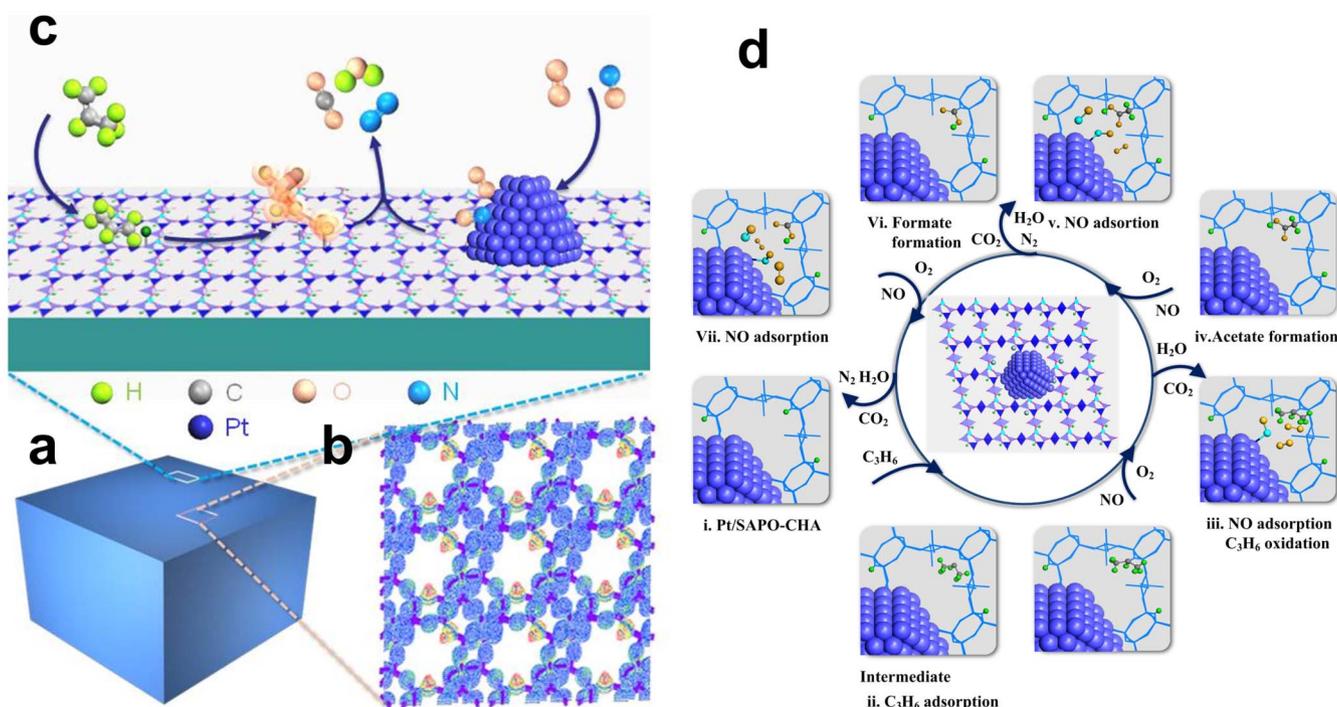
Figure 3 | Schematic representation for the effect of Brønsted acid sites on catalytic reactions of exhaust gases. (a) The particle of the SAPO-CHA crystal. (b) The simulated STM image of SAPO-CHA, showing high electron density (red) around the Brønsted acid site. (c) The activation of a propene molecule facilitated by the Brønsted acid site. (d) The proposed synergistic mechanism between the surface Brønsted acid sites and the Pt nanoparticles on the external surface of SAPO-CHA.

here, generally suffer from deactivation induced by the formation of coke inside the micropores. As expected, the thermogravimetric analysis (TGA) result reveals formation of coke (20 wt%) in the used Pt/SAPO-CHA catalyst (Fig. S11). Nevertheless, the conversions of CO, NO and C_3H_6 over Pt/SAPO-CHA at a space velocity of 34,000 mL gcat^{-1} h^{-1}, do not show any obvious decay over a 1,000-minute run at 620 K (in Fig. S12), suggesting that the coke formed during the catalytic reaction has no influence on activity of the Pt/SAPO-CHA catalyst. The NH_3-TPD (Fig. S13) and pyridine-TPD (Fig. S14) results suggest that coke forms only inside the micropores of SAPO-CHA and the amount of the Brønsted acid sites on the external surface is not varied. This observation well explains why the formation of coke leads to negligible deactivation as the Pt nanoparticles are mostly distributed on the external surface of the Pt/SAPO-CHA catalyst. On the other hand, it is exactly the Pt nanoparticles that catalyzes the complete transformation of propene to CO_2 and H_2O with concomitant NO reduction, and prevents the formation of coke on the external surface of the SAPO-CHA material.

Methods

Materials. All the reagents for synthesis and preparation were of analytic grade and used as received without further purification. Aluminum hydroxide and fumed silica were purchased from Aldrich. Phosphoric acid (85 wt%), hydrofluoric acid (40 wt%), cyclohexylamine and morpholine were all purchased from Shanghai Chemical Reagent Factory. γ-alumina (Al$_2$O$_3$ with a BET surface area of 200 m^2 g^{-1}) was provided by Beijing Chemical Factory.

Preparation of SAPO-CHA and AlPO-CHA. The SAPO-CHA precursor was synthesized by a hydrothermal method from the gel with a molar composition of 1.0cyclohexylamine: 0.5SiO$_2$: 1.0Al$_2$O$_3$: 0.9P$_2$O$_5$: 55H$_2$O following the procedure reported by Ashtekar et al[36]. Typically, 3.7 g of pseudoboehmite was first dispersed into 20 g of distilled water with stirring, followed by the addition of 0.75 g of fumed silica. After stirred at room temperature for one hour, 4.5 g of H$_3$PO$_4$ and then 3.6 g of cyclohexylamine were added slowly to the above mixture under vigorous stirring. After three hours, the resulting mixture was loaded to a Teflon-lined stainless steel autoclave and heated at 453 K for 10 days. The crystalline product was filtered off, washed with deionized water and dried at 333 K overnight. The as-synthesized

material was calcined at 873 K in air for 24 hours to remove the template. The molar ratio Si : Al : P of the obtained SAPO-CHA was estimated to be 1 : 4.3 : 3.5 from the XRF results.

For comparison, microporous AlPO-CHA without Brønsted acidity was also prepared hydrothermally from the gel with a molar composition of 1.0 morpholine: 1.0 Al$_2$O$_3$: 1.0 P$_2$O$_5$: 60 H$_2$O: 0.02 HF, following the procedure reported in the literature[37].

Loading of Pt. Pt was loaded onto SAPO-CHA, AlPO-CHA, and γ-Al$_2$O$_3$ by a modified wet impregnation method, leading to the formation of Pt/SAPO-CHA, Pt/AlPO-CHA, and Pt/Al$_2$O$_3$, respectively. Prior to the impregnation, SAPO-CHA and AlPO-CHA were calcined at 873 K in air for 24 hours to decompose the organic template within the micropores, while γ-Al$_2$O$_3$ was dried at 383 K for five hours to remove the physically adsorbed H$_2$O molecules and other species. A certain amount of H$_2$PtCl$_6$ was dissolved into 10 mL of ethanol. The calcined SAPO-CHA, AlPO-CHA, and γ-Al$_2$O$_3$ powders were then dispersed into the above ethanolic solution, respectively. These mixtures were kept at 333 K for two hours with vigorous stirring. Finally, Pt loaded samples, Pt/SAPO-CHA, Pt/AlPO-CHA, and Pt/Al$_2$O$_3$, were obtained by removal of the ethanol solvent with a rotary evaporator at 333 K. After dried at 383 K for 12 hours, the Pt loaded samples were sieved to 20–40 meshes. For comparison, a Pt/Al$_2$O$_3$ sample was also prepared through aging the Pt-impregnated Pt/Al$_2$O$_3$ at approximately 1173 K for five hours, and the corresponding sample was designated Pt/Al$_2$O$_3$-aging.

General characterization. The powder X-ray diffraction (XRD) patterns were recorded on a Rigaku Dmax-2200 diffractometer (Rigaku, Japan) with Cu Kα radiation (λ = 1.5418 Å). The distribution and crystal lattice of Pt were examined with a transmission electron microscope (JEM-2100F, JEOL, Japan), operating at 200 kV. The morphology of the samples was observed with a scanning electron microscope (SEM) (JEOL JSM-6700F, Japan), operated at 5 kV. Nitrogen adsorption/desorption analyses were performed on a Micromeritics ASAP 2010 M + C nitrogen adsorption instrument (Micrometritices Inc., USA) at 77 K. The contents of Pt loaded in the samples were determined by inductively coupled plasma spectroscopy (Thermo Electron Corporaton). Approximately 0.5 wt% Pt was loaded in the Pt/SAPO-CHA, Pt/AlPO-CHA, and Pt/Al$_2$O$_3$ samples.

Hydrogen temperature programmed reduction (H$_2$-TPR) of the samples was performed in a quartz tube reactor equipped with a thermal conductivity detector (TCD). 200 mg of sample was pretreated under He flow (50 mL min^{-1}) at 673 K for 30 min to remove the adsorbed water. After cooled to 323 K, the sample was exposed to a flow of 5% H$_2$/He (50 mL min^{-1}) and the temperature was raised to 1073 K at a rate of 10 K min^{-1}. The TPD experiments of adsorbed pyridine and NH$_3$ were performed in a quartz tube reactor equipped with a TCD. After saturated

with ammonia or pyridine, the samples were purged with pure He at 373 K for two hours. Then, the samples were heated to 973 K at ramp rate of 10 K min^{-1} under helium flow (50 mL min^{-1}). The FTIR spectra were recorded on a Bruker IFS 66 v/S FTIR spectrometer equipped with a deuterated triglycine sulfate (DTGS) detector.

The Pt L_3-edge X-ray absorption spectra (XAS) were obtained on the BL14W1 beamline at the Shanghai Synchrotron Radiation Facility (SSRF), operated at 3.5 GeV with injection currents of 140–210 mA. A Si (111) double-crystal monochromator was used to reduce harmonic component of the monochrome beam. All the samples were measured in fluorescence mode. The powder of a sample was pressed into a self-supporting disk, which was then sealed with Kapton membrane and subjected to XAS measurement. The IFEFFIT software was used to calibrate the energy scale, to correct the background signal and to normalize the intensity. Reliable parameters for the Z (Pt, Pt) and Z (Pt, O) contributions were determined by multiple-shell fitting in r space with application of k^3 and k^1 weightings in the Fourier transformations.

DFT calculations of the charge density around proton H$^+$ in SAPO-CHA. Calculations were carried out using the CASTEP periodic density functional theory (DFT) package. The exchange-correlation energy and potential were described self-consistently within the generalized gradient approximation (GGA-PW91). The self-consistent PW91 density was determined by iterative diagonalization of the Kohn−Sham Hamiltonian. The wave functions were expanded with the plane wave, and the ultra-soft pseudo-potential method was used to reduce the number of plane waves. Plane waves were used as a basis set with an energy cutoff of 340 eV .The electron density was approximated using a multipolar expansion up to hexadecapole. Typical overbinding associated with local density functionals was rectified through the use of the gradient-corrected Perdew-Burke-Ernzerhof (PBE) functional. The Brillouin-zone integration was performed using a $2 \times 2 \times 2$ Monkhorst–Pack (MP) grid. The STM images were simulated using the Tersoff–Hamann approach with a bias voltage of 2 V.

Evaluation of the catalytic property. The catalytic performance of the samples for purifying emission gases was evaluated in a fixed-bed reactor. Approximately 250 mg of the sample was loaded into a tube quartz reactor, and then was reduced *in situ* with the simulated feed gas, containing 0.82 vol% O_2, 0.12 vol% NO, 1.10 vol% CO, 0.08 vol% C_3H_6 and balance He at 673 K for two hours. After cooling to 303 K, the feed gas was allowed to pass through the reactor at a flow rate of 180 mL min^{-1} (corresponding to a space velocity of 43,200 mL h^{-1} gcat^{-1}). The effluent gas composition was analyzed on-line by two gas chromatographs (Shimadzu, GC-2014) equipped with a 5A column coupled with a thermal conductivity detector, and an Rtx-1 column coupled with a flame-ionization detector. Concentrations of NO$_x$ were determined by FTIR analyzer with Bruker IFS 66 v/S FTIR spectrometer, equipped with a quartz sample holder with CaF$_4$ windows.

1. Labinger, J. A. & Bercaw, J. E. Understanding and exploiting C-H bond activation. *Nature* **417**, 507–514 (2002).
2. Greeley, J. *et al.* Alloys of platinum and early transition metals as oxygen reduction electrocatalysts. *Nat. Chem.* **1**, 552–556 (2009).
3. Strmcnik, D. *et al.* Enhanced electrocatalysis of the oxygen reduction reaction based on patterning of platinum surfaces with cyanide. *Nat. Chem.* **2**, 880–885 (2010).
4. Kim, C. H., Qi, G., Dahlberg, K. & Li, W. Strontium-doped perovskites rival platinum catalysts for treating NO$_x$ in simulated diesel exhaust. *Science* **327**, 1624–1627 (2010).
5. Yamamoto, K. *et al.* Size-specific catalytic activity of platinum clusters enhances oxygen reduction reactions. *Nat. Chem.* **1**, 397–402 (2009).
6. Granger, P. & Parvulescu, V. I. Catalytic NO$_x$ abatement systems for mobile sources : from three-way to lean burn after-treatment technologies. *Chem. Rev.* **111**, 3155–3207 (2011).
7. Lok, B. M. *et al.* Silicoaluminophosphate molecular sieves: another new class of microporous crystalline inorganic solids. *J. Am. Chem. Soc.* **106**, 6092–6093 (1984).
8. Marcus, D. M. *et al.* Experimental evidence from H/D exchange studies for the failure of direct C-C coupling mechanisms in the methanol-to-olefin process catalyzed by HSAPO-34. *Angew. Chem., Int. Ed.* **118**, 3205–3208 (2006).
9. Haw, J. F. *et al.* The mechanism of methanol to hydrocarbon catalysis. *Acc. Chem. Res.* **36**, 317–326 (2003).
10. Wang, W., Buchholz, A., Seiler, M. & Hunger, M. Evidence for an initiation of the methanol-to-olefin process by reactive surface methoxy groups on acidic zeolite catalysts. *J. Am. Chem. Soc.* **125**, 15260–15267 (2003).
11. Boronat, M., Viruela, P. & Corma, A. Reaction intermediates in acid catalysis by zeolites: prediction of the relative tendency to form alkoxides or carbocations as a function of hydrocarbon nature and active site structure. *J. Am. Chem. Soc.* **126**, 3300–3309 (2004).
12. Tuma, C. & Sauer, J. Protonated isobutene in zeolites: *tert*-butyl cation or alkoxide. *Angew. Chem., Int. Ed.* **44**, 4769–4771 (2005).
13. Rozanska, X. *et al.* A periodic DFT study of isobutene chemisorption in proton-exchanged zeolites: dependence of reactivity on the zeolite framework structure. *J. Phys. Chem. B* **107**, 1309–1315 (2003).
14. Wang, J. *et al.* The influence of silicon on the catalytic properties of Cu/SAPO-34 for NO$_x$ reduction by ammonia-SCR. *Appl. Catal. B-Environ.* **27**, 137–147 (2012).
15. Martinez-Franco, R. *et al.* Rational direct synthesis methodology of very active and hydrothermally stable Cu-SAPO-34 molecular sieves for the SCR of NO$_x$. *Appl. Catal. B-Environ.* **127**, 273–280 (2012).
16. Fickel, D. W. *et al.* The ammonia selective catalytic reduction activity of copper-exchanged small-pore zeolites. *Appl. Catal. B-Environ.* **102**, 441–448 (2011).
17. Li, S., Falconer, J. L. & Noble, R. D. Improved SAPO-34 membranes for CO$_2$/CH$_4$ separations. *Adv. Mater.* **18**, 2601–2603 (2006).
18. Zhang, L. *et al.* Investigations of formation of molecular sieve SAPO-34. *J. Phys. Chem. C* **115**, 22309–22319 (2011).
19. Zhai, Y. *et al.* Alkali-stabilized Pt-OH$_x$ species catalyze low-temperature water-gas shift reactions. *Science* **329**, 1633–1636 (2010).
20. Cortes, J. M. *et al.* Comparative study of Pt-based catalysts on different supports in the low-temperature de-NO$_x$-SCR with propene. *Appl. Catal. B-Environ.* **30**, 399–408 (2001).
21. Borgna, A. *et al.* Sintering of Pt/Al$_2$O$_3$ reforming catalysts: EXAFS study of the behavior of metal particles under oxidizing atmosphere. *Catal. Lett.* **13**, 175–188 (1992).
22. Cho, I. H. *et al.* Investigation of Pt/γ-Al$_2$O$_3$ catalysts prepared by sol-gel method: XAFS and ethane hydrogenolysis. *J. Catal.* **173**, 295–303 (1998).
23. Wang, Q. Y. *et al.* The effect of La doping on the structure of Ce$_{0.2}$Zr$_{0.8}$O$_2$ and the catalytic performance of its supported Pd-only three-way catalyst. *Appl. Catal. B* **101**, 150–159 (2010).
24. He, H. *et al.* Pd-, Pt-, and Rh-loaded Ce$_{0.6}$Zr$_{0.35}$Y$_{0.05}$O$_2$ three-way catalysts: an investigation on performance and Redox properties. *J. Catal.* **206**, 1–13 (2002).
25. Guilhaume, N. & Primet, M. Three-way catalytic activity and oxygen storage capacity of perovskite LaMn$_{0.976}$Rh$_{0.024}$O$_{3 + \delta}$. *J. Catal.* **165**, 197–204 (1997).
26. Zhou, K. B. *et al.* Pd-containing perovskite-type oxides used for three-way catalysts. *J. Mol. Catal. A-Chem.* **189**, 225–232 (2002).
27. Papavasiliou, A. *et al.* An investigation of the role of Zr and La dopants into Ce$_{1-x-y}$Zr$_x$la$_y$O$_\delta$ enriched −Al$_2$O$_3$ TWC washcoats. *Appl. Catal. A* **383**, 73–84 (2010).
28. Farneth, W. E. & Gorte, R. J. Methods for characterizing zeolite acidity. *Chem. Rev.* **95**, 615–635 (1995).
29. Long, R. Q. & Yang, R. T. In situ FT-IR study of Rh-Al-MCM-41 catalyst for the selective catalytic reduction of nitric oxide with propylene in the presence of excess oxygen. *J. Phys. Chem. B* **103**, 2232–2238 (1999).
30. Santen, R. A. & Kramer, G. J. Reactivity theory of zeolitic broensted acidic sites. *Chem. Rev.* **95**, 637–660 (1995).
31. Wang, W. & Hunger, M. Reactivity of surface alkoxy species on acidic zeolite catalysts. *Acc. Chem. Res.* **41**, 895–904 (2008).
32. Xin, M., Hwang, I. C. & Woo, S. I. *In situ* FTIR study of the selective catalytic reduction of NO on Pt/ZSM-5. *Catal. Today.* **38**, 187–192 (1997).
33. perez-Ramirez, J. *et al.* Characterization and performance of Pt-USY in the SCR of NO$_x$ with hydrocarbons under lean-burn conditions. *Appl. Catal. B* **29**, 285–298 (2001).
34. Bamwenda, G. R. *et al.* Selective reduction of nitric oxide with propene over platinum-group based catalysts: studies of surface species and catalytic activity. *Appl. Catal. B* **6**, 311–323 (1995).
35. Captain, D. K. & Amiridis, M. NO reduction by propylene over Pt/SiO$_2$: An *in situ* FTIR study. *J. Catal.* **194**, 222–232 (2000).
36. Ashtekar, S., Chilukuri, S. V. V. & Chakrabarty, D. K. Small-pore molecular sieves SAPO-34 and SAPO-44 with chabazite structure: A study of silicon incorporation. *J. Phys. Chem.* **98**, 4878–4883 (1994).
37. Marchese, L. *et al.* AlPO-34 and SAPO-34 synthesized by using morpholine as templating agent. FTIR and FT-Raman studies of the host-guest and guest-guest interactions within the zeolitic framework. *Micropor. Mesopor. Mater.* **30**, 145–153 (1999).

Acknowledgments

Author contributions

W.F. and J.S.C. developed the idea and designed the experiments. W.F. performed the sample fabrication, measurements and data analysis. W.F., H.L.B., X.H.L., K.X.W., X.W., Y.Y.C. and J.S.C. analyzed the data, and discussed the results. W.F., X.H.L., K.X.W. and J.S.C. co-wrote the paper. J.S.C. planned and supervised the project.

Additional information

Supplementary information accompanies this paper at http://www.nature.com/scientificreports

Competing financial interests: The authors declare no competing financial interests.

How to cite this article: Fu, W. *et al.* Synergistic effect of Brønsted acid and platinum on purification of automobile exhaust gases. *Sci. Rep.* **3**, 2349; DOI:10.1038/srep02349 (2013).